# The Ocean's Role in Climate Change

# The Ocean's Role in Climate Change

By

Alexander Polonsky

Cambridge
Scholars
Publishing

The Ocean's Role in Climate Change

By Alexander Polonsky

This book first published 2019

Cambridge Scholars Publishing

Lady Stephenson Library, Newcastle upon Tyne, NE6 2PA, UK

British Library Cataloguing in Publication Data
A catalogue record for this book is available from the British Library



ISBN (10): 1-5275-2389-6
ISBN (13): 978-1-5275-2389-0

# TABLE OF CONTENTS

# ABBREVIATIONS AND DESIGNATIONS

ACI – Atmospheric Circulation Index

AMO – Atlantic Multidecadal Oscillation

AO – Arctic Oscillation

AR – Assessment Report (or Auto Regression in statistical assessments)

AT – Air Temperature

AT1000 – Absolute Topography of 1000 hPa Surface

ATLAS – Autonomous Temperature Line Acquisition System

CAA – Centers of Atmospheric Action

CMIP – Coupled Models Intercalibration Project

EAO – East Atlantic Oscillation

EC – European Commission

EM – Eurasian Mode

EOF – Empirical Orthogonal Functions

EOS – Equation of Sea Water

ENI – El Niño index

ENSO – El Niño-Southern Oscillation

EU – Equatorial Undercurrent

FP – Framework Programme (European Programme for Scientific Collaboration)

GAC – Global Atmospheric Circulation

GC – Guyana Current

GCM – Global Circulation Model

GHG – Greenhouse Gas

GISS – Goddard Institute for Space Studies (NASA Laboratory)

IGBP – International Geospheric-Biospheric Programme

IPCC – Intergovernmental Panel on Climate Change

ITCZ – Intertropical Convergence Zone

KE – Kinetic Energy

MBT – Mechanical Bathythermographs

MHT – Meridional Heat Transport

MWH – Monthly Waves Height

NAO – North Atlantic Oscillation

NADW – North Atlantic Deep Water

NASG – North Atlantic Subtropical Gyre

NCAR – National Center for Atmospheric Research

NCEP – National Center for Environmental Prediction

NEC – North Equatorial Currents

NECC – North Equatorial Countercurrents

NBC – North Brazil Current

NOAA – National Oceanic and Atmospheric Administration

NODC – National Oceanographic Data Centre

NH – Northern Hemisphere

NP – North Pacific Index

OHC – Ocean Heat Content

OWS – Ocean Weather Stations

PAM – Polar-Asian Mode

PDO – Pacific Decadal Oscillation

PIRATA – Prediction and Research Moored Array in the Atlantic

PMEL – Pacific Marine Environmental Laboratory

PSU – Practical Salinity Unit

RAMA – Research Moored Array for African-Asian-Australian Monsoon Analysis and Prediction

RCP – CMIP 5 Climate Project Scenarios

SAT – Surface Atmosphere Temperature

SEC – South Equatorial Currents

SECC – South Equatorial Countercurrent

SEOS – Science Education through Earth Observation for High Schools (FP6 Project)

SLP – Sea Level Pressure

SM – Scandinavian Mode

SOI – Southern Oscillation Index

SST – Sea Surface Temperature

Sv – Sverdrup ($10^6$ cubic meters per second)

TEOS – Thermodynamic Equation of Sea Water

TOGA – Tropical Ocean and Global Atmosphere

TOGA-TAO – TOGA Observational System for the Atmosphere and Ocean

TRITON – Triangle Trans-Ocean Buoy Network

UML – Upper Mixed Layer

UNFCCC – UN Framework Convention on Climate Change

WA – Wave Height Anomalies

WOCE – World Ocean Circulation Experiment

XBT – Expendable Bathythermograph

20CR – 20th Century Reanalysis

OX, OY, OZ – Axes in the Cartesian coordinate system (eastward, northward and downward in oceanography).

t – time.

$\overline{V_i} = \{\overline{U}, \overline{V}, \overline{W}\}$ – Components of the average velocity.

$\overline{U_i'} = \{u', v', w'\}$ or $\overline{U_i'} = \{U', V', W'\}$ – Fluctuations of velocity.

$g_i = \{0, 0, g\}$ – Gravitational acceleration.

$f = \{0, 2\Omega Cos\varphi, -2\Omega Sin\varphi\}$ – Coriolis components.

1 if i,j,k = 1,2,3 or if there are any even replacements relatively combination i,j,k = 1,2,3;

$\varepsilon_{ikl} = \{$ -1 if there are any odd replacements relatively combination i,j,k = 1,2,3;

0 if any indexes are repeated.

$\nu, \chi$ – Coefficients of molecular viscosity and heat exchange.

$\alpha = \left( \frac{1}{\rho_0} \frac{\partial \rho}{\partial T} \right)$ – Coefficient of thermal expansion.

$\rho$ – Density.

P – Pressure.

T – Temperature (or relative temperature against an abyssal temperature).

$\varepsilon = \nu \left( \frac{\overline{\partial u_i'}}{\partial x_j} \right)^2$ – Rate of dissipation in the locally-uniform turbulent flow.

$b = \frac{\left( \overline{u_i'} \right)^2}{2}$ – Intensity of turbulence (or kinetic energy of turbulence).

$\tau_{ij} = \overline{u_i' u_j'}$ (or $\tau_{ij} = \rho \overline{u_i' u_j'}$) – Reynolds stresses tensor.

$\overline{u_i' T'}, \overline{u_i' \rho'}$ – Turbulent fluxes of heat and density.

$\tau_{0x} = \rho_0 \overline{U' W'} \Big|_{z=0}$, $\tau_{0y} = \rho_0 \overline{V' W'} \Big|_{z=0}$ or $\tau_{0x} = \rho_0 \overline{u' w'} \Big|_{z=0}$, $\tau_{0y} = \rho_0 \overline{v' w'} \Big|_{z=0}$ – Tangential wind stresses at the surface.

$K_{z,,}$ , $K_{zT}$ – Coefficients of vertical turbulent exchange by momentum and heat.

$K_L$, $K_{LT}$ – Coefficients of horizontal turbulent exchange by momentum and heat.

$\alpha_T = \frac{K_{zT}}{K_z}$

$K_b$ – Coefficients of vertical turbulent diffusion (for kinetic turbulent energy).

$$\alpha_b = \frac{K_b}{K_z}$$

$K_0$ – Effective coefficient of vertical turbulent exchange in thermocline.

$V_* = (\tau_0/\rho_0)^{1/2}$

l – Turbulent scale in the UML.

h – UML thickness.

$T_0$ – UML temperature.

S – Salinity.

$R_i = \left[ \frac{g\alpha \partial \overline{T} / \partial z}{\left(\frac{\partial \overline{U}}{\partial z}\right)^2 + \left(\frac{\partial \overline{V}}{\partial z}\right)^2} \right]$ – Richardson number.

$R_f = \left[ \frac{g\alpha \overline{T'W'}}{\overline{U'W'}\frac{\partial \overline{U}}{\partial z} + \overline{V'W'}\frac{\partial \overline{V}}{\partial z}} \right]$ – Dynamic Richardson number.

$R_l$ - $\frac{U\lambda}{\nu}$ - Reynolds number (U – typical velocity, λ – typical scale).

χ - Karman constant.

$L_э = V_*/f$ – Ekman scale.

$L = V_*^3 / (g\alpha q_0)$ – Monin-Obukhov scale.

$N = L/L_э$ – Kazansky-Monin parameter.

$$G \equiv \int_0^h \left( \overline{U'W'} \frac{\partial \overline{U}}{\partial z} + \overline{V'W'} \frac{\partial \overline{V}}{\partial z} \right) \partial z + \overline{W' \left( b + \frac{p'}{\rho_0} \right)} \Big|_{я=0}$$

Integral rate of the production of turbulent energy within the UML.

$D \equiv \int_0^h \nu \left( \overline{\frac{\partial U_i'}{\partial x_j}} \right)^2 dz$ - Integral rate of the dissipation of turbulent energy within the UML.

# INTRODUCTION

Climate is a statistical ensemble of the states which characterizes the "ocean-atmosphere-lithosphere-cryosphere-biosphere" system over the course of a 30 year period (Monin, 1999). So, the term 'climate change' determines a change of different parameters in the climate system from one 30 year time interval to another (or others). It should be emphasized that the 4th and 5th IPCC Assessment Reports use the term 'climate change' to refer to natural internal processes or external forcing (such as modulations of the solar cycles, volcanic eruptions) and persistent anthropogenic changes in the composition of the atmosphere or in land use. This definition differs markedly from that of the UN Framework Convention on Climate Change (UNFCCC). Article 1 of the UNFCCC defines climate change as "a change of climate which is attributed directly or indirectly to human activity that alters the composition of the global atmosphere and which is in addition to natural climate variability observed over comparable time periods." Thus the UNFCCC makes a distinction between climate change, which is attributable to human activities altering the atmospheric composition, and climate variability, which is attributable to natural causes (IPCC 4th Assessment Report, 2007). In the present work, only the IPCC's definition of climate change is used. Despite the conditional character of this definition, it is used for its 30 year averaging system for the assessment of different climatic characteristics.

It should be noted that the conventional 30 year averaging of different parameters of the climate system implies an existence of some peculiarities in the spectra of these parameters in the vicinity of the 30 year periodicity, for instance a reduced energy. In this case, the processes accounting for the climate change (i.e. the processes with periodicities exceeding 30 years) are explicitly separated from the processes accounting for the climate characteristics themselves. Higher frequency fluctuations (such as regular seasonal and daily variations, synoptic fluctuations, etc.) are inherent characteristics of the climate, while lower frequency variations (such as the Atlantic Multidecadal Oscillation (AMO) or Pacific Decadal Oscillation (PDO)) account for climate change (Fig. I.1, upper

panel). If such peculiarities are absent then the choice of a 30 year averaging of climate system parameters is not clear. For instance, for the parameter represented in the lower spectrum of Fig. I.1 below, a 2 year averaging period would be more reasonable.

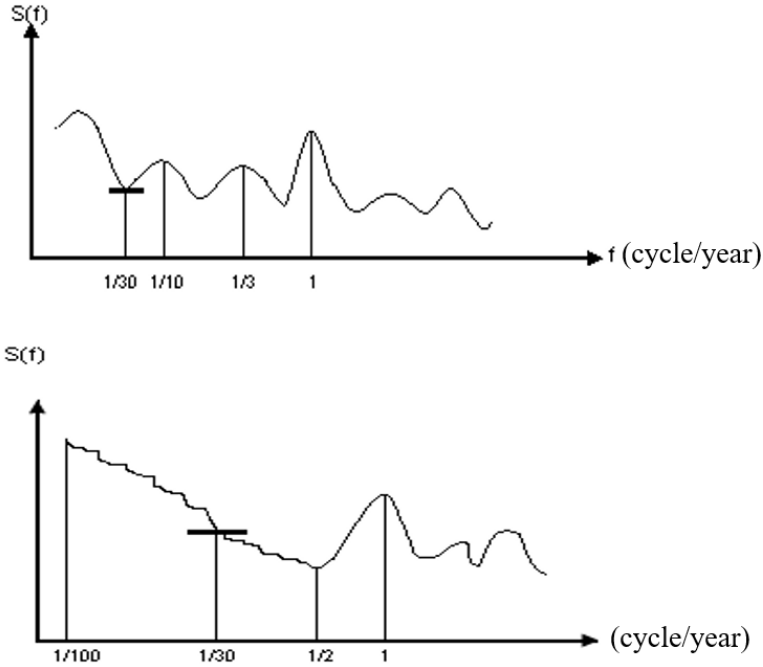


Fig. I.1. Schematic spectrum of any parameter of the climate system classified under the 'climate change' definition. Upper panel: spectrum with a power minimum at the frequency of 1/30 cycles per year. Lower panel: 'red' spectrum with a frequency of between 1/100 and 1/2 cycles per year. The thick horizontal line denotes the frequency of 1/30 cycles per year (after Polonsky, 2008a).

What do we know about the typical spectra of the parameters of the climate system? Unfortunately, long-term instrumental data to calculate the spectrum by resolving variations with periodicities ranging from a few hours to a few hundred years are absent. That is why one uses proxy-data and/or long-term simulation outputs for spectral assessments. Their accuracy cannot be guaranteed, however, and different experts doubt that estimated spectra are reliable. The problem of the accuracy of spectra assessed using proxy-data can be demonstrated using the results published

by von Storch and his co-authors (2004). The authors of this paper showed that the magnitude of natural climate variabilities estimated using noisy and rather short-term proxy-data can be underestimated by a factor of up to two or three. The principal cause of such underestimations is the redness of the spectrum (i.e. a concentration of the fluctuations' power in the low frequency spectral band), which is often ignored when the proxy-data are processed. The quality of the numerical simulations of climate change is not always sufficient because of the rather coarse resolution and poor parameterization of some sub-grid processes. However, some useful conclusions concerning the typical climatic spectra can be drawn using proxy-data and/or long-term simulation outputs. For instance, recently Parsons et al. (2017) analyzed the results of long-term ensemble simulations and proxy-data all over the globe and in selected regions of the World Ocean. They have shown that in some regions (such as Niño-3.4 in the Equatorial Pacific) the interannual variability prevails, while in other ones (such as the North and South Atlantic) the multidecadal variations are more powerful (see Fig. I.2). There are some significant peaks in the spectra of the interannual-to-multidecadal periods in different regions. However, the global peculiarity in the spectra of temperature in the vicinity of a periodicity of about 30 years is absent. It is only present in some subregions of the Atlantic-European region (as will be shown below). It should be noted that the spectral estimations of simulation outputs and proxy-data in agree one with one another in general in some regions, but disagree in other ones. This is a result of the poor simulation of some processes in the climate system. One of the disadvantageous consequences of this is the underestimation of the role of natural low-frequency processes in the coupled ocean-atmosphere system in the climate scenario assessments.

Thus, a 30 year averaging period for different parameters of the system should generally be considered as conventional. In fact, it is a compromise between longer-term (century-scale) averaging (which is too large for most climatic parameters, taking into account the restriction of time series) and shorter-term (a few years) averaging (which is acceptable from a statistical point of view, but otherwise seems too short and its use would lead to a dramatic increase of climatic variability because of the high-amplitude interannual fluctuations).

The 4$^{th}$ and 5$^{th}$ Assessment Reports of the Intergovernmental Panel on Climate Change (IPCC 4$^{th}$ Assessment Report, 2007; Climate Change, 2014) insisted that long-term tendencies of variations in sea level air temperature (AT), humidity, cloudiness, precipitation, snow and ice in the 20$^{th}$ and 21$^{st}$ centuries are mostly due to the anthropogenic forcing of the

climatic system. The most intense low-tropospheric warming occurs in the high latitudes of the Northern Hemisphere (NH). The mean annual NH air temperature has increased by more than 1°C in the 20th and early 21st centuries. However, this increase was not monotonic. A fast increase in AT occurred between 1910 and 1940 and in the last third of the 20th century, while in the mid-20th century a tropospheric cooling was observed. Since the last years of the 20th century, the rise in AT has been interrupted again. This is the so-called 'global warming hiatus'. Numerous published results (e.g. Shlesinger and Ramankutty, 1994; Kushnir, 1994; Voskresenskaya and Polonsky, 1994, 2004; Dellworth et al., 2000; Polonsky, 2008a, b; Knight et al., 2010; Semenov et al., 2010; Trenbert, 2010; and many others) show that natural multidecadal fluctuations of the ocean-atmosphere parameters (including the meridional heat flux (MHT)) in the Atlantic and Pacific Oceans have caused such temporal variability in AT. Thus, the observed climate fluctuations are anthropogenic climate changes together with a superimposed natural variability of the coupled ocean-atmosphere system. The existence of trend-like anthropogenic global warming and the superimposed quasi-periodical multidecadal variability of the coupled ocean-atmosphere system mean it is necessary to distinguish between climate change's artificial and natural origins. Without this, a correct assessment of climatic tendencies for the forthcoming decades is impossible (Polonsky, 2008a, 2015). In other words, an answer to the following question is crucial. What are the relative roles of external (natural and anthropogenic) and internal factors in climate change? It should be remembered that the former are due to changes of insolation, tidal activity and anthropogenic forcing, while the latter are due to inherent climatic variability, including the interactions between different components of the climate system.

Satellite observations show that the interannual-to-interdecadal change in globally averaged solar insolation at the upper stratosphere boundary is about 0.1% (Hoffert et al., 1999). This change does not have a crucial impact on the interannual-to-interdecadal variability of the meteorological characteristics of the low troposphere. For instance, the spectral assessments of the variations of surface meteorological parameters over an 11 year period using a long-term time series, generalized by Monin (1999), show that statistically significant fluctuations can be extracted in no more than 20% of the total analyzed cases. So, there is quite a weak, although not negligible, climate signal induced by the solar cycle, which is confirmed by some recent results (Dunstone et al., 2016; Gray et al., 2013).

climatological terms at the end of the 1990s (Mantua et al., 1997; Gershunov and Barnett, 1998) as a quasi-periodical alternation of warm and cool surface waters in the Pacific Ocean, north of 20°N. During a 'warm' (or 'positive') PDO phase, the west Pacific becomes cool and part of the eastern ocean warms; during a 'cool' (or 'negative') phase, the opposite pattern occurs. Just two full PDO cycles in the past century have been found and described by different authors, namely the 'cold' PDO regimes of 1890-1924 and 1947-1976, and the 'warm' PDO regimes which prevailed from 1925 to 1946 and from 1977 to the end of the 1990s.

Minobe (1997) has shown that 20$^{th}$ century PDO fluctuations were concentrated in two general bands of periodicity, one from 15-25 years and the other from 50-70 years. PDO phase changes are of significant importance for the global climate as they impact hurricane activity in the Pacific and Atlantic oceans, droughts and floods, marine ecosystems state, and global air temperature.

**Table 2.3: El Niño / La Niña episodes (after Polonsky et al., 2012a)**

| El Niño | | La Niña | |
|---|---|---|---|
| **Year** | **Month** | **Year** | **Month** |
| 1957 | 12 | 1964 | 12 |
| 1958 | 1, 2 | 1965 | 1, 2 |
| 1965 | 12 | 1970 | 12 |
| 1966 | 1, 2 | 1971 | 1, 2 |
| 1972 | 12 | 1973 | 12 |
| 1973 | 1, 2 | 1974 | 1, 2 |
| 1982 | 12 | 1975 | 12 |
| 1983 | 1, 2 | 1976 | 1, 2 |
| 1987 | 12 | 1988 | 12 |
| 1991 | 12 | 1989 | 1, 2 |
| 1992 | 1, 2 | 1998 | 12 |
| 1994 | 12 | 1999 | 1, 2 |
| 1995 | 1 | 1999 | 12 |
| 1997 | 12 | 2000 | 1, 2 |
| 1998 | 1, 2 | 2007 | 12 |
| 2002 | 12 | 2008 | 1, 2 |
| 2009 | 12 | 2008 | 2 |
| 2010 | 1, 2 | 2010 | 12 |

The other option for the assessment of the PDO index is to calculate the leading EOF of SST in the North Pacific. The associated time coefficient can be used as a measure of the PDO. A distinctive feature of the corresponding atmospheric pattern is a basin-scale area of negative/positive SLP anomalies between 30-60ºN and positive/negative SLP anomalies centered at 50ºN over the Rockies. It is characterized by any of the several indices calculated from the SLP field over the North Pacific region. One of these is the North Pacific (NP) index (the mean SLP anomaly over the central North Pacific; see Trenberth and Hurrell, 1994). It should be emphasized that the North Pacific Oscillation described in earlier papers (Rogers, 1981) is associated with the second Pacific SST EOF, not with the leading one (i.e. the PDO; see Yeh et al., 2011).

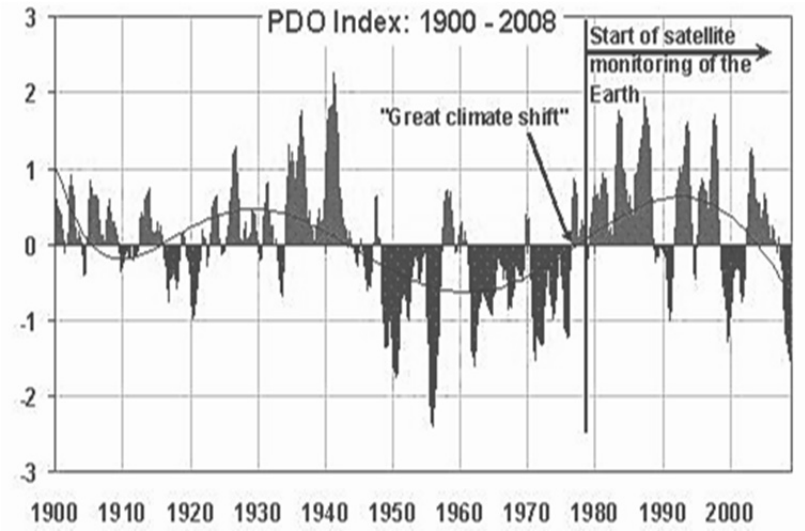


Fig. 2.46. The PDO index time series from 1900-2008. The arrow points to the climate shift of 1976, which is associated with a change of the PDO's phase. The start of the satellite era in the late 1970s is shown by the bold vertical line (adopted from www.cpc.ncep.noaa.gov/products).

There are different explanations for the PDO's origin. The prevailing hypotheses are that the PDO is caused by a 'reddening' of ENSO-induced forcing combined with stochastic atmospheric forcing (Newman et al., 2003) and advective processes in the North Pacific (mostly in the Pacific Subtropical gyre). At the same time, PDO has a modulating influence on the ENSO (Gershunov and Barnett, 1999). Some publications (e.g. Yeh et

al., 2011) show that different mechanisms can be more or less important in different periods of the 20th and 21st centuries. A recent publication by Newman et al. (2016) confirms the multimechanistic nature of the PDO. In any case, it mostly regards the inherent Pacific mode (Frankignoul et al., 2017).

Several mechanisms have been proposed to account for how the disturbances, induced by warm/cold SST Tropical Pacific anomalies, spread over the globe. One of them is an atmospheric bridge connecting the North Pacific and Atlantic oceans through the Northern Pole. There is a little evidence of the reality of such mechanisms. For example, Polonsky et al. (2012b) showed that the PDO significantly impacts the parameters of Mediterranean cyclones. Figures 2.47, 2.48 and 2.49 clearly demonstrate the impact of the PDO on cyclones' characteristics all over the Northern Hemisphere. Ding et al. (2017) found different European manifestations of the PDO for various La Niña types.

Thus, it can be concluded that not only the Atlantic interannual-to-interdecadal variability (such as the NAO and AMO), but also the Pacific interannual-to-interdecadal modes (above all the ENSO and PDO) effectively impact the meteorological parameters of the European-Mediterranean region. Impacts from both the Atlantic and the Pacific are detected in this region at a significant level (although the Atlantic signals are usually more significant).

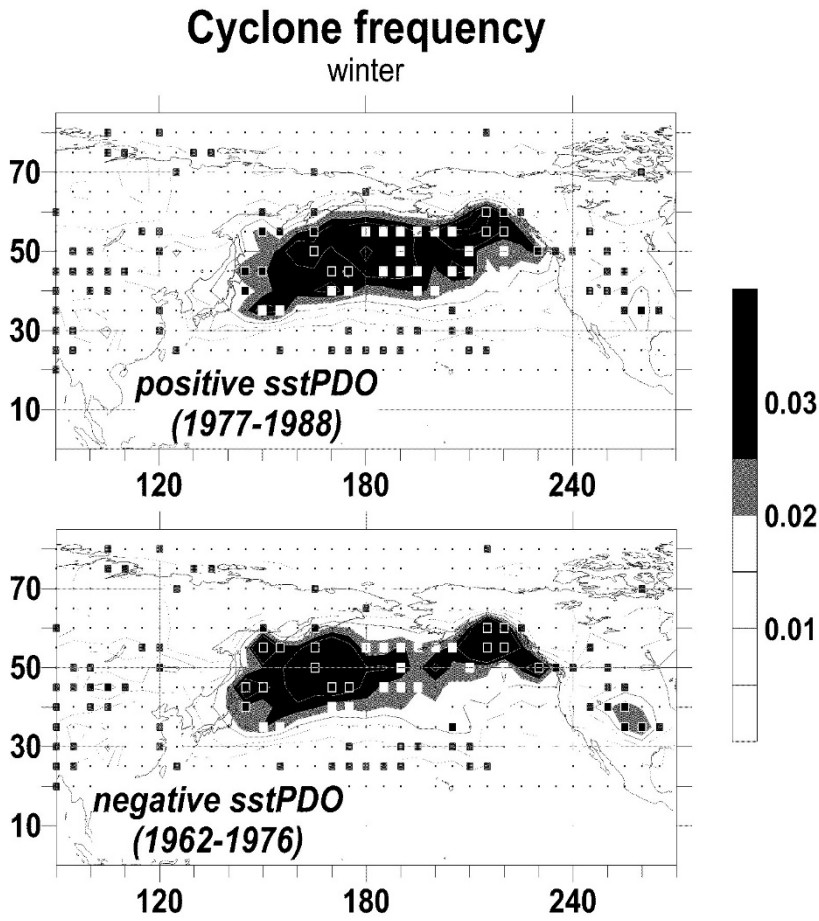


Fig. 2.47. Relative frequency (fraction; 0.01=1%) of cyclone centers in 5° grid cells in positive (top) and negative (bottom) PDO phases (composites); for the legend, see Fig. 2.27.

### 2.5.3 Indo-ocean Dipole and its Impact on the Eurasian Meteorological Fields

The Indo-ocean dipole (IOD) is quasi-periodic interannual SST variability in the Equatorial Indian Ocean. From the very beginning, the IOD was described as the principal interannual Indo-ocean mode (Saji et al., 1999). Since then, different authors have showed that some ENSO events generate a significant Indo-ocean response which manifests itself (among other ways) in the IOD (Fig. 2.50; Meyers et al., 2007; Roxy et al., 2011; Guo et al., 2015). However, sometimes the ENSO events do not generate the IOD. In these cases, the IOD arises as an internal Indo-ocean mode which can impact the Pacific Ocean variability (Ashok et al., 2003; Behera and Yamagata, 2003). This type of IOD has been observed especially frequently since the mid-1970s (Du et al., 2013). As showed by Polonsky et al. (2008), this is probably due to the difference in the season of the ENSO's generation. The canonical ENSO is a spring event, while a non-canonical ENSO causes a few months' delay. As a result, the Indo-ocean equatorial currents are principally reorganized and prevent the spread of westward equatorially-trapped waves (which are a principal cause of the IOD).

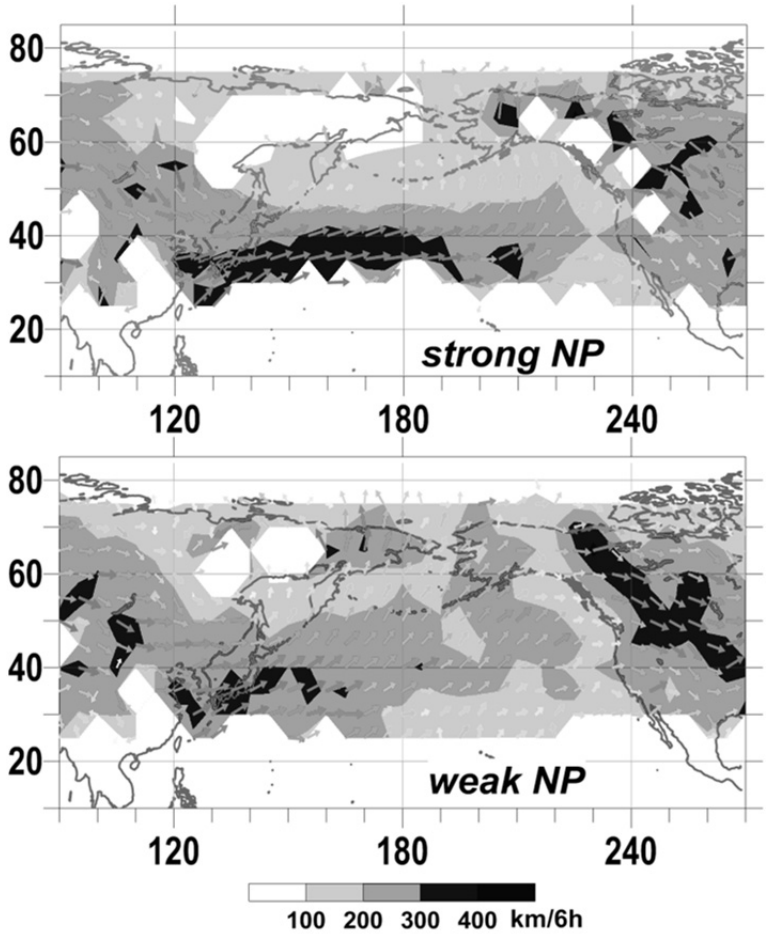


Fig. 2.48. Winter cyclone velocity (as in Fig. 2.30) in the strong (top) and weak (bottom) NP phases.

It should be emphasized that the Indo-ocean interannual variability interacts not only with the Pacific (above all with the ENSO) but also with other large-scale climatic modes, such as the North Atlantic Oscillation (Polonsky et al., 2004b, 2008; Feliks et al., 2013; Fletcher and Cassou, 2015). Moreover, the IOD-ENSO interaction can account for generation of the most intense El Niños (the so-called super El Noños, see Saji et al., 2018). Therefore, the separation of the regional manifestations of Indian

Ocean variations (such as the IOD) and other climate signals using observational data is a complicated problem. General circulation models (GCMs) are useful tools to solve this problem. In particular, the atmospheric response to IOD events, prescribed as SST anomalies, can answer the question of regional manifestations of Indo-ocean anomalies. There are numerous publications devoted to the description of ocean-induced atmospheric response and associated regional anomalies, especially concerning ENSO events (see e.g. Molteni, 2003; Bulic and Kucharski, 2012; Semenov et al., 2012; Polonsky, 2015; and many others). However, this is not the case for the IOD-related SST anomalies. A recent paper by Polonsky and Basharin (2017) is an exception. The authors carried out an ensemble set of numerical experiments using the IOD-related SST anomalies (Fig.2.51) to force the GSM SPEEDY and compared the simulation results with Eurasian composites and EOFs extracted from the reanalyses.

In the negative IOD phase, significant positive SAT anomalies in Eastern Europe (with their center in the northwestern part of the Black Sea region) and in the Far East were identified. At the same time, there is an area (with its center over northern Iran), where a significant negative SAT anomaly occurs. A second area with negative SAT anomalies occurs over Western Europe. Further SAT anomalies are significant over Scandinavia (Fig. 2.52). The structure of the simulated response resembles the results of the statistical analysis described earlier for the region under consideration and it proves the significance of the IOD events' influence on the SAT variability in the Eurasian region in summertime.

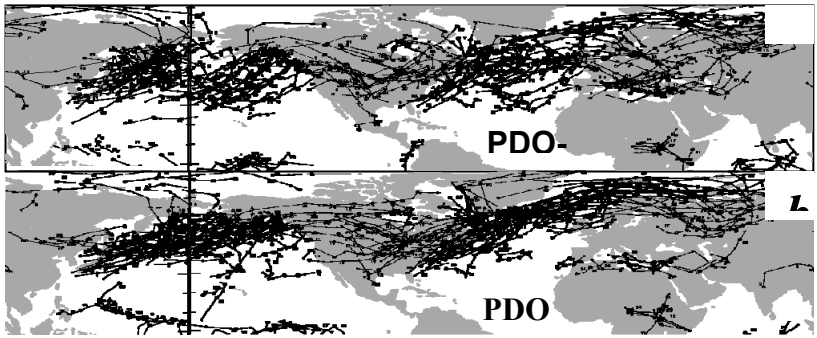


Fig. 2.49. Trajectory of January cyclones in the Northern Hemisphere for the negative AMO phase (1967-1992) and different PDO phases: (a) PDO- and (b) PDO+ (Polonsky et al., 2012b).

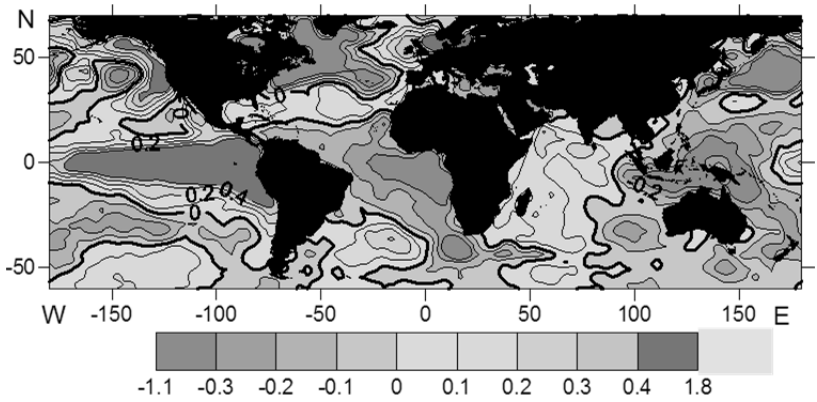


Fig. 2.50. The global summer composite of SST anomalies in the positive IOD phase.

Sensitivity experiments showed that the typical magnitude of SAT anomalies in the European and Far East regions is about 0.5□ per 1.0□ of SST anomalies in the Tropical Indian Ocean. Taking into account that the magnitude of large-scale Indian Ocean SST anomalies reaches about 1.5□ for a typical individual IOD event, one can estimate the typical SAT response for the Eastern Mediterranean as between 0.5-1.0□. Of course, this assessment is obtained without the effect of ocean-atmosphere coupling which (in principle) can be important for the interannual climate variations in the Indo-ocean (Iizuka et al., 2000) and Atlantic-European (Bulic and Kucharski, 2012) regions. Note that the simulated spatial pattern of the SAT anomalies over Eurasia shown in Fig. 2.52 is quite stable and does not change notably between the 10$^{th}$ and 30$^{th}$ modeling years.

The mechanism of SST-induced teleconnection in principle is well-known. It involves the modification of the Hadley/Walker cell, the jet stream, parameters of transient eddies and planetary Rossby waves (Rodwell and Hoskins, 1996; Polonsky et al., 2004a). There are numerous publications describing different European-Mediterranean manifestations of Atlantic, Pacific and Indo-ocean interannual-to-interdecadal modes (such as the NAO, ENSO, IOD, AMO and PDO). Some of them are quite robust, others are not. The signal-to-noise ratio varies from one mode to another. Besides this, the characteristics of these modes are changing in the warming climate. However, one can conclude that the principal oscillation modes have an effective impact on the hydrometeorological parameters of the European-Mediterranean region. Eastern European and

Black Sea manifestations of the global climatic processes will be considered in the next chapter.

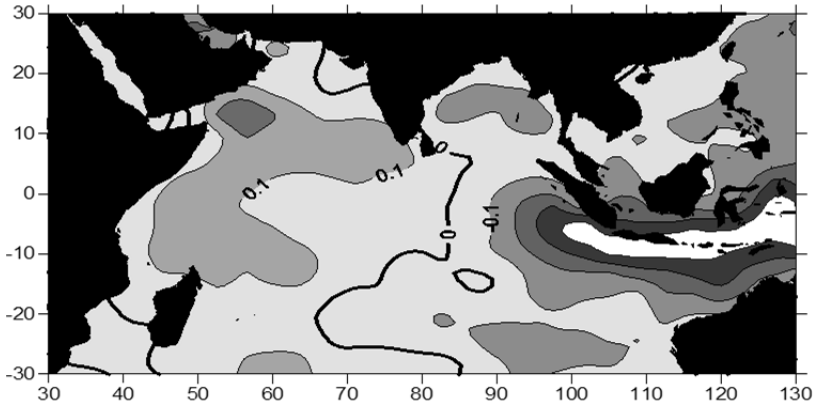


Fig. 2.51. The global summer composite of SST anomalies in the positive IOD phase for the Indo-ocean region used for the forcing of the GCM SPEEDY by Polonsky and Basharin (2017). The negative composite is the same, but multiplied by -1.

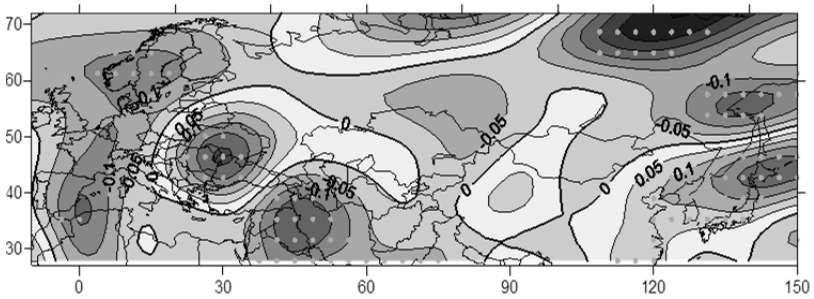


Fig. 2.52. The simulated ensemble difference in summer mean surface air temperature in the negative and positive IOD phases over the Eurasia region after 30 years of integration. Areas with significant values (with a 90% confidence level) are dotted in green (after Polonsky and Basharin, 2017).

# CHAPTER THREE

# REGIONAL METEOROLOGICAL AND MARINE MANIFESTATIONS OF GLOBAL WARMING AND NATURAL OCEAN-ATMOSPHERE PROCESSES IN EASTERN EUROPE AND THE BLACK SEA BASIN

## 3.1. Variability of Black Sea Cyclones and Anticyclones Associated with North Atlantic Signals

The synoptic variability of the atmospheric characteristics has an essential impact on the circulation and structure of the Black Sea waters. Thus, the predominance of cyclonic vorticity in the wind field formed over the Black Sea in winter and the corresponding wind circulation intensification are explained purely by the synoptic variations. The predominance of anticyclones in summer not only changes the sign of vorticity in the wind field but is also accompanied by an elevation of the inflow of short-wave solar radiation (caused by the decrease in cloudiness) and a weakening of the turbulent heat fluxes (due to the wind weakening). As a result, the heat gained by the sea surface not only increases, it also affects the circulation and water structure. However, the role of the synoptic processes in the formation of the water structure and circulation in the Black Sea is not restricted to the indicated effects. In fact, the synoptic processes play the role of the main source of momentum and mechanical energy transferred from the atmosphere into the sea. This follows from the fairly simple considerations published about 50 years ago (Monin, 1969). Indeed, since the dependence of tangential friction stresses on the sea surface on wind velocity is non-linear, the monthly average momentum fluxes are largely (by more than 50%) formed by storms. Strong storms accompanying deep cyclones, the frequency of which is quite low, are of special importance in this sense. The numerical analyses of the circulation of the Black Sea waters, carried out using different models, confirm this observation (Shapiro, 1998; Staneva, 2005).

The characteristics of cyclones and anticyclones in the European-Mediterranean region not only undergo significant changes on the seasonal scale; interannual and decadal variations connected, in particular, with the NAO and AMO are also readily detected (see Chapter 2). Hence, the low-frequency variations of the statistical characteristics of synoptic atmospheric processes (including the parameters of deep cyclones) caused by the NAO and AMO determine the interannual and decadal variations of the circulation and structure of the Black Sea waters.

In the present section, I estimate the basic characteristics of cyclones and anticyclones in the Black Sea region for all four seasons according to the NCEP reanalysis data for 1952-2000 and study their correlation with the NAO and AMO using the published results of Polonsky et al. (2007). In the subsequent subsections, these results will be used to explain the observed low-frequency variations of the hydrophysical and hydrochemical characteristics of the Black Sea.

To describe the interannual-to-decadal synoptic signals over the Black Sea basin, the NCEP reanalysis data for 1952-2000 (for the synoptic terms 0000 and 1200 GMT on a grid of 2.5 × 2.5°) have been used. The procedure of processing the data was discussed in Chapter 2. The quality of the reanalysis data was discussed in detail at specialized conferences (see e.g. Proceedings, 1998; 2000). It was demonstrated that these data can be used for a reliable analysis of synoptic processes with characteristic horizontal scales of about 1000 km. The Atlantic cyclones and anticyclones satisfy this condition. At the same time, the Mediterranean and Black Sea cyclones are smaller than the Atlantic cyclones and some of their parameters cannot be reliably identified on the indicated, relatively coarse grid. Most likely, the area of small cyclones is evaluated with the lowest accuracy because their sizes only slightly exceed the area of the squares used to evaluate their parameters. For the same reason, the depths of Mediterranean and Black Sea cyclones may be underestimated. Therefore, the presented data on the variability of the sizes of the cyclones should be regarded as an upper boundary and the values of the depths of the cyclones as a lower boundary. However, the frequency (recurrence) of synoptic formations and its variations are evaluated with sufficiently high accuracy. This is confirmed (at least partially) by the fact that the frequency of cyclones in the Black Sea region evaluated according to the reanalysis data decreased sharply between the 1960s-90s (see below), despite the permanent improvement of the systems of observations capable (especially after the beginning of specialized satellite measurements in the late 1970s) of the detection of even quite small eddy structures. Hence,

more exact identification of small synoptic disturbances in the 1950s-70s would only lead to insignificant improvements to the obtained estimates.

The reanalysis data were studied for all four seasons. December, January and February were regarded as winter months, March, April and May as spring months, and so forth. The characteristics of cyclones and anticyclones averaged over the entire Black Sea region (37.5-50°N, 27.5-45°E) have been evaluated. To establish the dependence of the characteristics of cyclones and anticyclones on the NAO phase, we applied the composites method. For the NAO index, we used the standardized time coefficient of the first empirical mode in the expansion of the monthly fields of surface pressure in the North Atlantic region with the following coordinates: 10-80°N and 20-80°W. First, we chose 20 months for each season at both ends of the ranked sample. Then the characteristics of the synoptic eddies for each square were averaged separately over each month and year for the years with high and low NAO indices (for winter, these indices are presented in Table 3.1). The average values (composites) obtained for these two groups of months and years were compared with an aim to extract the NAO-induced signal. The composite significance was evaluated by using different statistical criteria for different characteristics (the same method as in Chapter 2). The statistical characteristics of cyclones and anticyclones do not obey the normal distribution law (Bardin and Polonsky, 2005). Therefore, to analyze the most intense cyclones, we used the data for 25% of the most intense atmospheric eddies.

The spectral estimates were obtained by using nonparametric methods. The periodograms evaluated according to a three-month series with daily resolution were smoothed by using the Parzen window and then confidence intervals were estimated. The Parzen window is one of the methods applied that strongly decreases the variance of sample estimates and, hence, deteriorates the frequency characteristics of the spectra (Jenkins and Watts, 1969). This method was deliberately chosen because our aim was to estimate the number of significant peaks in certain fairly broad frequency ranges.

The analysis of frequency of cyclones observed in the Black Sea region reveals the following basic features (Fig. 3.1). From the second half of the 1960s to the late 1980s and mid-1990s, winter cyclones became more than three times more infrequent. Moreover, the frequency (recurrence) of cyclones also significantly decreased in spring and autumn. However, the absolute value of the linear trend in these periods of the year was about 2-3 times smaller than in winter. Generally speaking, these trends are also observed for 25% of the most intense cyclones (dashed lines in Fig. 3.1).